



Communication

The Enhanced Thermal Stability of $(\text{Mg}_{0.95}\text{Ni}_{0.05})_2\text{TiO}_4$ Dielectric Ceramics Modified by a Multi-Phase Method

Chun-Hsu Shen ^{1,*}, Ting-Wei Shen ², Tsai-Yu Hsieh ¹, Kai-Chun Lan ¹, Shen-Hsien Hsu ¹, Ching-Hsuan Wang ¹, Yu-Ting Lin ³, Wen-Fang Wu ² and Zong-Liang Tseng ^{3,*}

¹ Department of Electronic Engineering, Ming Chuan University, Taoyuan City 333, Taiwan

² Department of Mechanical Engineering, National Taiwan University, Taipei 106, Taiwan

³ Department of Electronic Engineering and Organic Electronics Research Center, Ming Chi University of Technology, New Taipei City 243, Taiwan

* Correspondence: chshen0656@mail.mcu.edu.tw (C.-H.S.); zlltseng@mail.mcut.edu.tw (Z.-L.T.)

Abstract: The thermal stability of $(\text{Mg}_{0.95}\text{Ni}_{0.05})_2\text{TiO}_4$ dielectric ceramics has been improved by mixing with CaTiO_3 phases owing to higher positive temperature coefficients. The pure $(\text{Mg}_{0.95}\text{Ni}_{0.05})_2\text{TiO}_4$ and the mixture phase systems of CaTiO_3 -modified $(\text{Mg}_{0.95}\text{Ni}_{0.05})_2\text{TiO}_4$ were verified by XRD diffraction patterns to ensure the crystallite of different phases. The microstructures of the CaTiO_3 -modified $(\text{Mg}_{0.95}\text{Ni}_{0.05})_2\text{TiO}_4$ were observed by SEM and EDS to investigate the relation between element ratios and grains. As a result, it can be seen that the thermal stability of the CaTiO_3 -modified $(\text{Mg}_{0.95}\text{Ni}_{0.05})_2\text{TiO}_4$ can be effectively enhanced, compared with the pure $(\text{Mg}_{0.95}\text{Ni}_{0.05})_2\text{TiO}_4$. Moreover, the radio frequency dielectric performances of CaTiO_3 -modified $(\text{Mg}_{0.95}\text{Ni}_{0.05})_2\text{TiO}_4$ dielectric ceramics are strongly dependent upon the density and the morphology of the specimens. The champion sample with the ratio of $(\text{Mg}_{0.95}\text{Ni}_{0.05})_2\text{TiO}_4$ and CaTiO_3 of 0.92:0.08 showed an ϵ_r value of 19.2, an Qf value of 108,200 GHz, and a τ_f value of -4.8 ppm/ $^\circ\text{C}$, which may encourage $(\text{Mg}_{0.95}\text{Ni}_{0.05})_2\text{TiO}_4$ ceramics to broaden the range of novel applications and match the requirements of 5G or next-generation communication systems.

Keywords: thermal stability; radio frequency; dielectric ceramic



Citation: Shen, C.-H.; Shen, T.-W.; Hsieh, T.-Y.; Lan, K.-C.; Hsu, S.-H.; Wang, C.-H.; Lin, Y.-T.; Wu, W.-F.; Tseng, Z.-L. The Enhanced Thermal Stability of $(\text{Mg}_{0.95}\text{Ni}_{0.05})_2\text{TiO}_4$ Dielectric Ceramics Modified by a Multi-Phase Method. *Materials* **2023**, *16*, 2997. <https://doi.org/10.3390/ma16082997>

Academic Editor: Dong-Joo Kim

Received: 19 March 2023

Revised: 1 April 2023

Accepted: 6 April 2023

Published: 10 April 2023



Copyright: © 2023 by the authors. Licensee MDPI, Basel, Switzerland. This article is an open access article distributed under the terms and conditions of the Creative Commons Attribution (CC BY) license (<https://creativecommons.org/licenses/by/4.0/>).

1. Introduction

As a result of the continuous evolution of science and technology, millimeter-wave technology has been extensively developed and considered as a branch of 5G communication or next-generation mobile communication technology. Due to a large amount of data transmission, a multilayer board is required as the main circuit board design, leading to materials which should possess both low dielectric loss and conductor loss characteristics [1–5]. Dielectric materials, to date, are a good choice for creating high-frequency components that have a higher dielectric constant (ϵ_r), which can contribute to the miniaturization of components; high-quality factors (Qf values) can improve the energy of stored electromagnetic waves and the temperature coefficient of the resonance frequency (τ_f) approaching zero, which can enhance the thermal stability of the components. For example, when a filter possesses the three abovementioned characteristics, the filter results in effective downsizing, lower dielectric loss rates, greater filtering activity, and greater stability, unaffected by the external ambient temperature [6,7].

The ceramic systems based on MgTiO_3 have always received considerable attention and applications in the literature. For example, dielectric passive components of MgTiO_3 in a communication system have been employed to be a resonator, duplex, filter, and antenna [8–12]. Therefore, it is considerably important to enhance the dielectric performance of MgTiO_3 . When the ratio of Mg and Ti is 2:1, the binary titanate ceramic Mg_2TiO_4 possesses a spinel-type structure that belongs to the cubic phase with Fd-3m space group (2 2 7). It demonstrates an ϵ_r value of 14, a Qf value of 150,000 GHz, and a τ_f value

of -50 ppm/ $^{\circ}\text{C}$ [13–15]. In addition, to further improve the dielectric characteristics, the method of partial substitution that selects Ni^{2+} (0.069 nm) with a radius resembling Mg^{2+} (0.078 nm) to perform the substitution was presented [16]. When the Mg^{2+} ions were replaced by Ni^{2+} ions to form $(\text{Mg}, \text{Ni})_2\text{TiO}_4$ compositions, the $(\text{Mg}_{0.95}\text{Ni}_{0.05})_2\text{TiO}_4$ compositions possessing a spinel-type structure presented a good dielectric performance with an ϵ_r value of 16.43, a Q_f value of 238,000 GHz, and a τ_f value of -55 ppm/ $^{\circ}\text{C}$ [17]. Moreover, an inferior $(\text{Mg}_{0.95}\text{Ni}_{0.05})\text{TiO}_3$ phase also appeared during the synthesizing of $(\text{Mg}_{0.95}\text{Ni}_{0.05})_2\text{TiO}_4$, which may be attributed to the effect of the thermal decomposition mechanism [18]. However, the slight $(\text{Mg}_{0.95}\text{Ni}_{0.05})\text{TiO}_3$ -doped $(\text{Mg}_{0.95}\text{Ni}_{0.05})_2\text{TiO}_4$ possess a comparable performance, with an ϵ_r value of 17.2, a Q_f value of 180,000 GHz, and a τ_f value of -45 ppm/ $^{\circ}\text{C}$ [19], compared to those of the pure $(\text{Mg}_{0.95}\text{Ni}_{0.05})_2\text{TiO}_4$ composition [17].

On the other hand, a multi-phase method has been employed to modify the dielectric characteristics. In Mg_2TiO_4 – SrTiO_3 systems [20], Mg_2TiO_4 and SrTiO_3 have spinel cubic (lattice parameters: $a = 8.439$ Å, space group $\text{Fd}3\text{m}$) (ICDD-PDF#00-003-0858) and cubic perovskite (ICDD-PDF#01-084-0443), respectively. When x increased, the peak intensity of SrTiO_3 increased and the lattice parameters of Mg_2TiO_4 remained unchanged, which demonstrates that the two-phase system was used to modify relative permittivity in the Mg_2TiO_4 – SrTiO_3 system. In $(\text{Mg}_{0.95}\text{Zn}_{0.05})_2\text{TiO}_4$ – SrTiO_3 systems [21], the lattice parameters had slight influence and remained unchanged after the SrTiO_3 was added into $(\text{Mg}_{0.95}\text{Zn}_{0.05})_2\text{TiO}_4$, which confirms that the presence of a two-phase system could effectively promote densification in the $(\text{Mg}_{0.95}\text{Zn}_{0.05})_2\text{TiO}_4$ matrix. In addition, CaTiO_3 - and SrTiO_3 -modified $(\text{Mg}_{0.95}\text{Co}_{0.05})_2\text{TiO}_4$ ceramics [22,23] were presented using a multi-phase method for low-loss dielectric properties at microwave frequencies. Furthermore, thermal stability of dielectric ceramics is another important factor in practical applications. However, few studies have been conducted to discuss the thermal stability of $(\text{Mg}_{0.95}\text{Ni}_{0.05})_2\text{TiO}_4$. For this purpose, we have made great efforts to enhance the thermal stability factor of $(\text{Mg}_{0.95}\text{Ni}_{0.05})_2\text{TiO}_4$ compositions using a perovskite structured SrTiO_3 additive to form a two-phase system in our previous report [24].

In this study, we demonstrate the microstructure and radio frequency dielectric characteristics of the CaTiO_3 -modified $(\text{Mg}_{0.95}\text{Ni}_{0.05})_2\text{TiO}_4$ ceramic system for enhancing its thermal stability factor using the multi-phase method. We attempted to add CaTiO_3 with a high positive temperature coefficient to form a three-phase system and to compensate the negative temperature coefficient of $(\text{Mg}_{0.95}\text{Ni}_{0.05})_2\text{TiO}_4$. X-ray diffraction (XRD), scanning electron microscopy (SEM), and energy-dispersive X-ray spectrometer (EDS) analyses were also employed to study the microstructure grain boundary, and compositions of the ceramic system. The radio frequency dielectric performances of the CaTiO_3 -modified $(\text{Mg}_{0.95}\text{Ni}_{0.05})_2\text{TiO}_4$ were quantified and examined by employing the formation of multi-phase coexistence.

2. Materials and Method

In this study, $(\text{Mg}_{0.95}\text{Ni}_{0.05})_2\text{TiO}_4$ and CaTiO_3 were produced by a mixed-oxide solid-state reaction using the following high-purity chemical powders: magnesium oxide (MgO), nickel oxide (NiO), calcium carbonate (CaCO_3), and titanium dioxide (TiO_2). Because MgO is hygroscopic in nature, it first removes the moisture remaining at 600 $^{\circ}\text{C}$ for 2 h. The mixture of the above oxides was mixed according to the stoichiometries of $(\text{Mg}_{0.95}\text{Ni}_{0.05})_2\text{TiO}_4$ and CaTiO_3 . They were then ball ground in distilled water (ball grinding medium) for 24 h. All mixed powders were parched in a kiln and pre-phased (calcine) at 1100 $^{\circ}\text{C}$ for 4 h in a high-temperature furnace. Then, the pre-phased reagents were mixed again according to the chemical molar ratio of $(1-x)(\text{Mg}_{0.95}\text{Ni}_{0.05})_2\text{TiO}_4 \cdot x\text{CaTiO}_3$, and ball ground into a fine powder for 24 h. Then, polyvinyl alcohol (PVA 500; Showa, Tokyo, Japan) as a binder was added to the calcined powder, uniformly granulated, screened with a 100-mesh screen, and compressed with a pressure of 200 MPa to form a tablet form with a height of 0.5 cm and diameter of 1.1 cm. The sintering temperatures of the tablets were set at 1300 – 1425 $^{\circ}\text{C}$ for 4 h in air. The risen and dropped temperature rates were set at 10 $^{\circ}\text{C}/\text{min}$ for all samples.

The crystallization-phase observation of the pre-phased powder and mixture compositions were analyzed by XRD (Rigaku D/Max III. V., Tx for USA) The lattice constant was calculated using the Rietveld method to fit the XRD patterns. SEM (Philips XL-40FEG, Eindhoven, The Netherlands) was employed to observe the surface morphologies of samples, and EDS was utilized to demonstrate the different phases and compositions. The apparent densities of the samples were measured using the Archimedes method. The ϵ_r and Q_f values at radio frequencies were measured by the Hakki–Coleman dielectric resonator method [25–27].

The measurement was mainly composed of a vector network analyzer (HP8757D, Agilent Technologies, Taipei, Taiwan) and sweep oscillator connections (HP8350B, Agilent Technologies, Taipei, Taiwan). The thermal stability (τ_f values) was evaluated with a temperature range from 20 to 80 °C. The following Formula (1) was utilized to obtain the τ_f value (ppm/°C):

$$\tau_f = \frac{f_2 - f_1}{f_1(T_2 - T_1)} \quad (1)$$

where f_1 and f_2 represent the resonant frequencies at T_1 and T_2 , respectively.

3. Results and Discussion

Figure 1 presents the XRD patterns of the $(1-x)(\text{Mg}_{0.95}\text{Ni}_{0.05})_2\text{TiO}_4 \cdot x\text{CaTiO}_3$ with an x value of 0.08 after sintering at different temperatures for 4 h. According to the JCPDS card, a three-phase system can be observed, which consisted of $(\text{Mg}_{0.95}\text{Ni}_{0.05})_2\text{TiO}_4$ phase with a spinel-type structure as the primary crystalline phase (Mg_2TiO_4 , ICDD–PDF#00-025-1157; lattice constants $a = b = c = 0.84409$ nm), $(\text{Mg}_{0.95}\text{Ni}_{0.05})\text{TiO}_3$ phase (MgTiO_3 , ICDD–PDF#00-006-0494), and a CaTiO_3 phase with perovskite structure (JCPDS #22-0153). The lattice constant was slightly decreased with the increasing sintering temperature ($a = b = c$ from 0.84005 to 0.83456 nm), indicating sharper main peaks of the $(\text{Mg}_{0.95}\text{Ni}_{0.05})_2\text{TiO}_4$ phase and larger grain size. No other obvious phases and impurities were identified in Figure 1. In addition, the reason for the presence of the $(\text{Mg}_{0.95}\text{Ni}_{0.05})\text{TiO}_3$ phase is generally considered to be the uneven particle size of the initial materials, which increases the probability of secondary crystallization nucleation. Another reason for the formation of the $(\text{Mg}_{0.95}\text{Ni}_{0.05})\text{TiO}_3$ phase may be the effect of the thermal decomposition mechanism [18]. However, the ratio of $(\text{Mg}_{0.95}\text{Ni}_{0.05})\text{TiO}_3$ phase in the ceramics was decreased due to the increased grain boundary motion with the increasing sintering temperature, as shown in Table 1. Moreover, the $(\text{Mg}_{0.95}\text{Ni}_{0.05})\text{TiO}_3$ had no noticeable impact on the dielectric properties of $(\text{Mg}_{0.95}\text{Ni}_{0.05})_2\text{TiO}_4$ in our previous study [19]. Therefore, the influence of the inferior $(\text{Mg}_{0.95}\text{Ni}_{0.05})\text{TiO}_3$ phase can be negligible when the sintering temperature is over 1350 °C.

Figure 2 presents the results of the XRD analysis of the $(1-x)(\text{Mg}_{0.95}\text{Ni}_{0.05})_2\text{TiO}_4 \cdot x\text{CaTiO}_3$ with different x values. It can be observed that the different contents have no obvious influence on the phase growth of the $(\text{Mg}_{0.95}\text{Ni}_{0.05})_2\text{TiO}_4$. A few $(\text{Mg}_{0.95}\text{Ni}_{0.05})\text{TiO}_3$ peaks still existed in all patterns. As mentioned above, the effect of the inferior $(\text{Mg}_{0.95}\text{Ni}_{0.05})\text{TiO}_3$ phase on dielectric performance is quite slight and can be neglected. The lattice constant of the $(\text{Mg}_{0.95}\text{Ni}_{0.05})_2\text{TiO}_4$ with a different amount of the CaTiO_3 contents is presented in Table 2. It was also observed that all samples have a spinal cubic structure with the lattice constants ($a = b = c$) from 0.84005 to 0.83456 nm, indicating that the $(\text{Mg}_{0.95}\text{Ni}_{0.05})_2\text{TiO}_4$ is still in the primary phase. When CaTiO_3 was blended with $(\text{Mg}_{0.95}\text{Ni}_{0.05})_2\text{TiO}_4$, no obvious influence on the lattice constants of $(\text{Mg}_{0.95}\text{Ni}_{0.05})_2\text{TiO}_4$ could be found (Table 2). Furthermore, the growth of mixed phases in the one ceramic may cause a negative effect due to structural dissimilarities and the larger ionic radii values of Ca^{2+} (0.106 nm) compared to those of Mg^{2+} (0.078 nm) and Ni^{2+} (radii = 0.069 nm) [16]. However, the XRD analysis confirms the coexistence of the multiple phases without the structural dissimilarities in our samples.

Figure 3 shows the SEM images of the morphologies of the $0.92 \cdot (\text{Mg}_{0.95}\text{Ni}_{0.05})_2\text{TiO}_4 \cdot 0.08 \text{CaTiO}_3$ sintered at different temperatures. When the sintering temperature was increased, the

grain size increased in Figure 3a–f, which is consistent with the XRD results (Figure 1). The pores reduced with the sintering temperature increasing from 1300 to 1350 °C. The reason for the increase in the grain size and the decrease in pores is the thermal drive energy, which enables connection and expands the neck between the grains. Therefore, Figure 3a–c exhibits the grain growth with better movement of the grain boundary and a more uniform and dense morphology. However, when the sintering temperature was increased from 1350 to 1425 °C, the grain size still increased, and the pore size became larger. This is attributed to the excessive extrusion between grains and air pressure under too-high sintering temperatures, which is similar with previous reports [20–24]. Furthermore, grains of $0.92 \cdot (\text{Mg}_{0.95}\text{Ni}_{0.05})_2\text{TiO}_4 \cdot 0.08\text{CaTiO}_3$ can be roughly divided into three shapes, as shown in Figure 3c. The EDS results of each grain are summarized in Table 3. Therefore, the different grains were identified as follows: spot A is $(\text{Mg}_{0.95}\text{Ni}_{0.05})\text{TiO}_3$; spot B is $(\text{Mg}_{0.95}\text{Ni}_{0.05})_2\text{TiO}_4$ and spot C is CaTiO_3 . The EDS results are consistent with the XRD analysis, verifying that the $(1-x) (\text{Mg}_{0.95}\text{Ni}_{0.05})_2\text{TiO}_4 \cdot x\text{CaTiO}_3$ is a three-phase coexistence system.

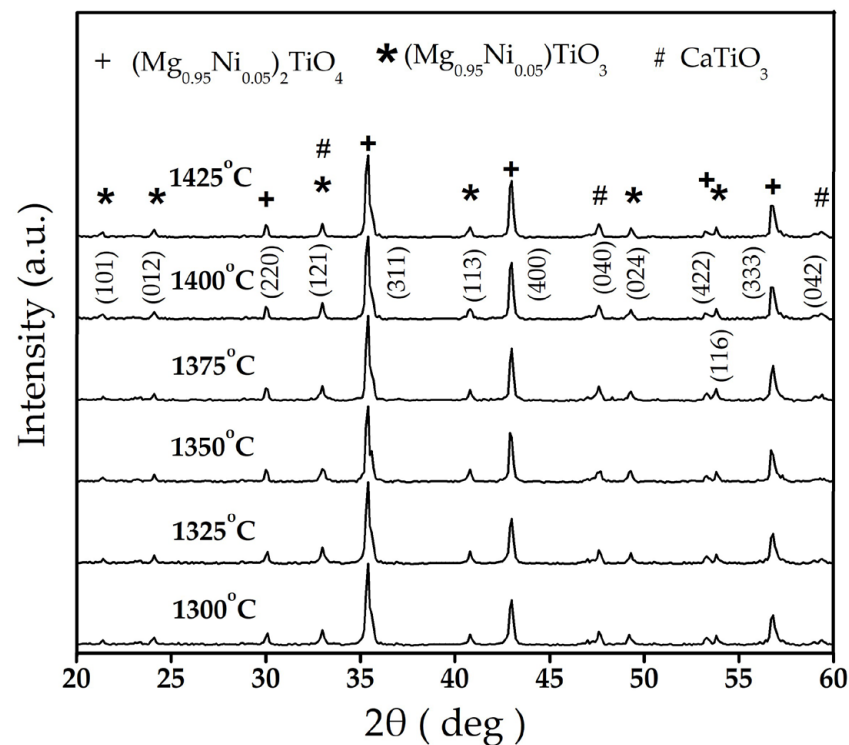


Figure 1. X-ray diffraction patterns of $0.92 \cdot (\text{Mg}_{0.95}\text{Ni}_{0.05})_2\text{TiO}_4 \cdot 0.08\text{CaTiO}_3$ sintered at different temperatures for 4 h.

Table 1. The lattice parameter and compositions of $0.92 \cdot (\text{Mg}_{0.95}\text{Ni}_{0.05})_2\text{TiO}_4 \cdot 0.08\text{CaTiO}_3$ sintered at different temperatures for 4 h. $(\text{Mg}_{0.95}\text{Ni}_{0.05})\text{TiO}_3$ and CaTiO_3 ratios are determined by all peak areas of each phase.

Temperatures	a = b = c (nm)	$(\text{Mg}_{0.95}\text{Ni}_{0.05})\text{TiO}_3$ Ratio (%)	CaTiO_3 Ratio (%)
1300	0.84005 ± 0.1033	17.4	11.6
1325	0.84005 ± 0.1033	17.2	13.4
1350	0.83986 ± 0.0972	17	13.5
1375	0.83456 ± 0.0995	14.9	13.8
1400	0.83456 ± 0.0995	14.7	13.8
1425	0.83456 ± 0.0995	14.4	14.1

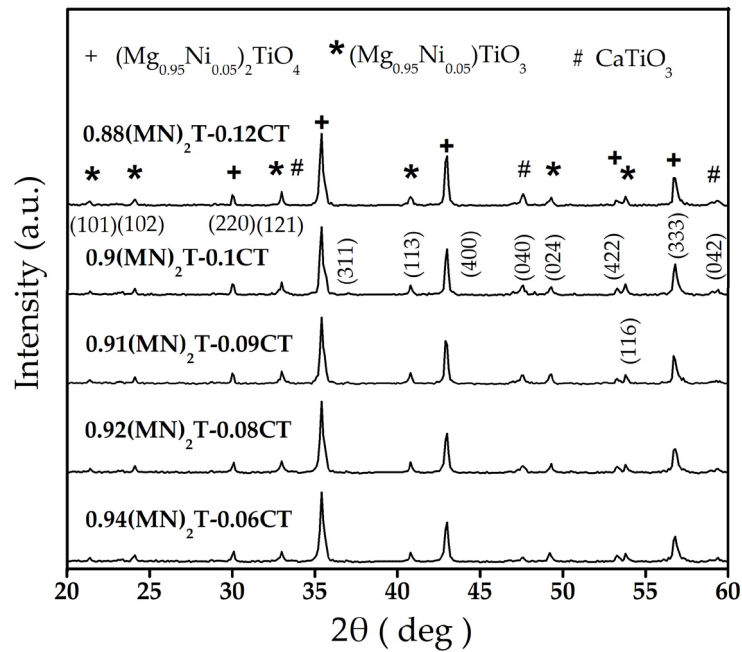


Figure 2. X-ray diffraction patterns of $(1-x)(\text{Mg}_{0.95}\text{Ni}_{0.05})_2\text{TiO}_4 \cdot x\text{CaTiO}_3$ sintered at 1350 °C for 4 h.

Table 2. The lattice parameter and compositions of $(1-x)(\text{Mg}_{0.95}\text{Ni}_{0.05})_2\text{TiO}_4 \cdot x\text{CaTiO}_3$ sintered at 1350 °C for 4 h. $(\text{Mg}_{0.95}\text{Ni}_{0.05})\text{TiO}_3$ and CaTiO_3 ratios are determined by all peak areas of each phase.

x Values	a = b = c (nm)	$(\text{Mg}_{0.95}\text{Ni}_{0.05})\text{TiO}_4$ Ratio (%)	CaTiO_3 Ratio (%)
0.06	0.84005 ± 0.1033	17.1	9.6
0.08	0.84005 ± 0.1033	17	13.5
0.09	0.83986 ± 0.0972	14.5	13.5
0.1	0.83456 ± 0.0995	13.3	13.7
0.12	0.83456 ± 0.0995	14	14.4

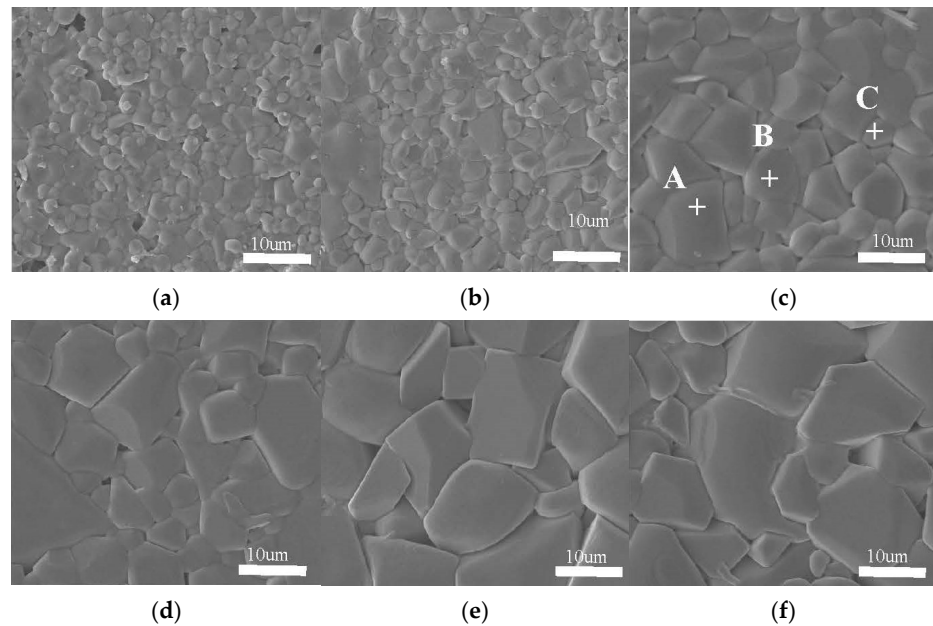
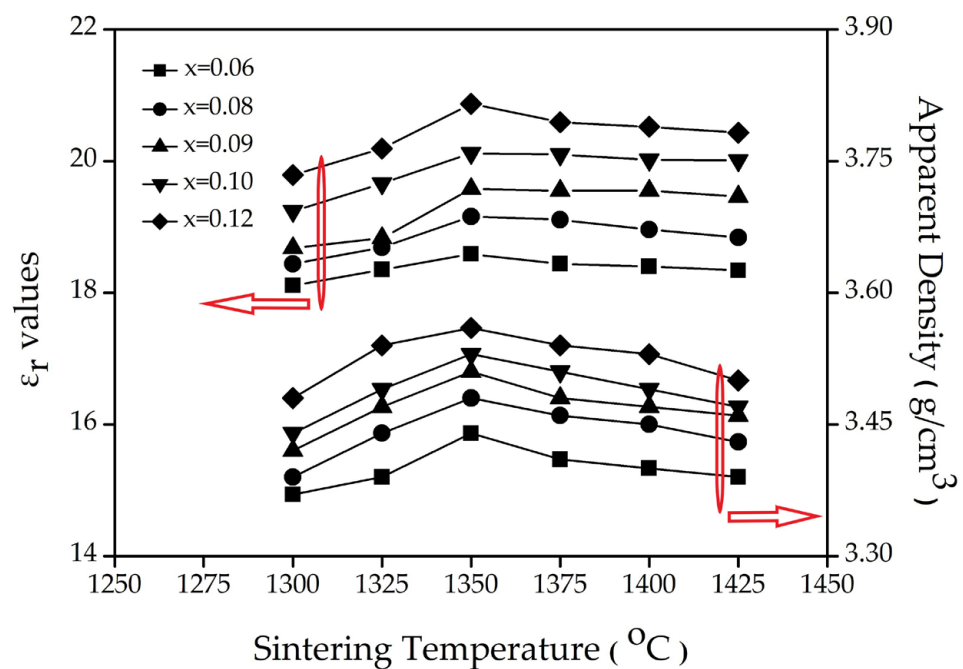


Figure 3. SEM images of $0.92 \cdot (\text{Mg}_{0.95}\text{Ni}_{0.05})_2\text{TiO}_4 \cdot 0.08\text{CaTiO}_3$ sintered at (a) 1300, (b) 1325, (c) 1350, (d) 1375, (e) 1400, and (f) 1425 °C for 4 h.

Table 3. Composition analysis from EDS results for spot A, B, and C in Figure 3c.

Spot	Atom (%)				
	Mg	Ni	Ca	Ti	O
A	17.54	2.2	0	16.84	63.42
B	24.27	2.25	0	19.51	53.97
C	0	0	20.42	19.49	60.09

Figure 4 shows the results of the apparent density and dielectric constant (ϵ_r values) of the $(1-x)(\text{Mg}_{0.95}\text{Ni}_{0.05})_2\text{TiO}_4 \cdot x\text{CaTiO}_3$ with different x values and temperatures. The apparent density was increased with the increasing x value because CaTiO_3 ($\sim 4.036 \text{ g/cm}^3$) possesses a higher density than that of $(\text{Mg}_{0.95}\text{Ni}_{0.05})_2\text{TiO}_4$ ($\sim 3.49 \text{ g/cm}^3$) [17]. Moreover, the apparent density value increased when the temperature increased from 1300 to 1350 °C, which is due to the grain growth (Figure 3a–c). However, the apparent density was reduced due to the enlarged pore size (Figure 3d–f) when the temperature increased from 1350 to 1425 °C. These results lead to the optimal sintering temperature of 1350 °C being obtained. Due to much higher dielectric constant (ϵ_r) of $(\text{Mg}_{0.95}\text{Ni}_{0.05})_2\text{TiO}_4$ (~ 16.4) and CaTiO_3 (~ 170) than that of air (~ 1), the ϵ_r of the $(1-x)(\text{Mg}_{0.95}\text{Ni}_{0.05})_2\text{TiO}_4 \cdot x\text{CaTiO}_3$ correlates positively with apparent density. Therefore, the ϵ_r changed with the change in the apparent density and the x value. Therefore, the dielectric constant changes from 18.6 to 20.9 as x increases from 0.06 to 0.12, as shown in Table 4.

**Figure 4.** The apparent density and dielectric constant (ϵ_r values) of the $(1-x)(\text{Mg}_{0.95}\text{Ni}_{0.05})_2\text{TiO}_4 \cdot x\text{CaTiO}_3$ sintered at different temperatures.**Table 4.** Microwave dielectric performances of $(1-x)(\text{Mg}_{0.95}\text{Ni}_{0.05})_2\text{TiO}_4 \cdot x\text{CaTiO}_3$ at 1350 °C for 4 h.

x Values	Density (g/cm^3)	ϵ_r Values	Q_f Values (GHz)	τ_f Values ($\text{ppm}/^\circ\text{C}$)
0.06	3.44	18.6	131,000	−20.7
0.08	3.48	19.2	108,200	−4.8
0.09	3.51	19.6	90,000	1.3
0.1	3.53	20.1	75,000	13.9
0.12	3.56	20.9	58,000	30.5

Figure 5 shows that the Qf value (quality factor) of the $(1-x)(\text{Mg}_{0.95}\text{Ni}_{0.05})_2\text{TiO}_4 \cdot x\text{CaTiO}_3$ decreased with the increasing the x value. It is attributed to the fact that the Qf value of CaTiO_3 (~3600 GHz) was relatively smaller than that of $(\text{Mg}_{0.95}\text{Ni}_{0.05})_2\text{TiO}_4$ (~238,000 GHz). In addition, the Qf of the $(1-x)(\text{Mg}_{0.95}\text{Ni}_{0.05})_2\text{TiO}_4 \cdot x\text{CaTiO}_3$ rises at 1300–1350 °C and drops at 1350–1425 °C in Figure 5. Compared with Figure 4, the Qf of the $(1-x)(\text{Mg}_{0.95}\text{Ni}_{0.05})_2\text{TiO}_4 \cdot x\text{CaTiO}_3$ correlated positively with the ϵ_r and apparent density. Although there are many factors that impact the Qf , such as dielectric loss (which is caused by the second phase), oxygen vacancy, grain size, and porosity [28], the Qf is mainly dependent on the apparent density in our case. Similar with the results of the apparent density at different temperatures (Figure 4), the Qf also reached the optimal value at 1350 °C, as listed in Table 4. The τ_f of the $(1-x)(\text{Mg}_{0.95}\text{Ni}_{0.05})_2\text{TiO}_4 \cdot x\text{CaTiO}_3$ sintered at different temperatures seems to maintain a constant value, which is strongly dependent on the CaTiO_3 contents (x value), as shown in Figure 5 and Table 4. The composition and phase determined the thermal stability of the $(1-x)(\text{Mg}_{0.95}\text{Ni}_{0.05})_2\text{TiO}_4 \cdot x\text{CaTiO}_3$ because a high positive temperature coefficient of CaTiO_3 can compensate the negative temperature coefficient of $(\text{Mg}_{0.95}\text{Ni}_{0.05})_2\text{TiO}_4$. Therefore, the τ_f was changed from -20.7 to 30.5 (ppm/°C) when x increased from 0.04 to 0.12, indicating that $\tau_f = 0$ is possible after controlling x . It is worth noting that the τ_f was only -4.8 ppm/°C at $x = 0.08$ but the Qf was kept at 108,200 GHz.

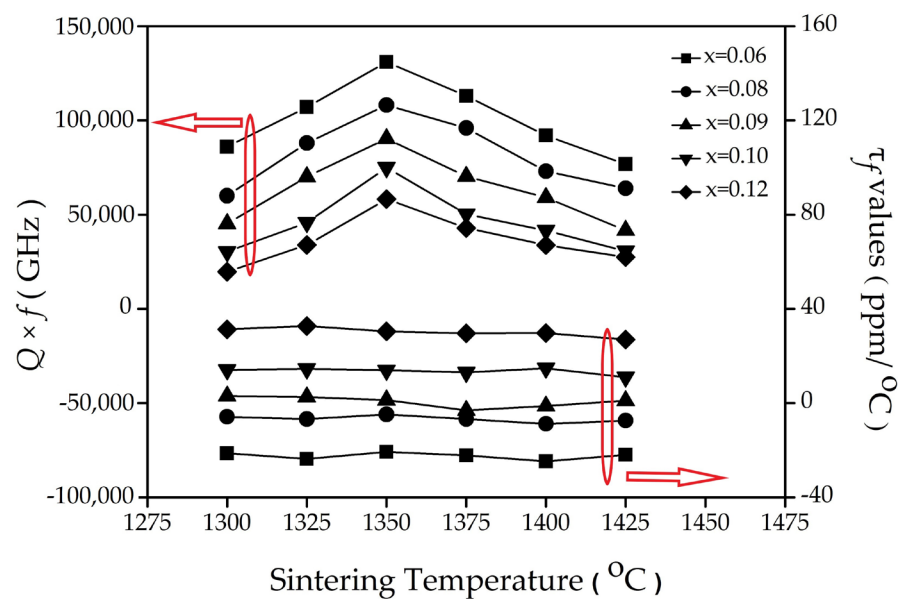


Figure 5. Qf and τ_f values of the $(1-x)(\text{Mg}_{0.95}\text{Ni}_{0.05})_2\text{TiO}_4 \cdot x\text{CaTiO}_3$ sintered at different temperatures for 4 h.

4. Conclusions

In conclusion, the thermal stability of the CaTiO_3 -modified $(\text{Mg}_{0.95}\text{Ni}_{0.05})_2\text{TiO}_4$ ceramic system was investigated. The dense morphology without pores can be obtained at 1350 °C, resulting in the optimal sintering temperature of the apparent density, ϵ_r , and Qf . A high positive temperature coefficient of CaTiO_3 can be used to improve the thermal stability of $(\text{Mg}_{0.95}\text{Ni}_{0.05})_2\text{TiO}_4$. The τ_f can be adjusted with changing the CaTiO_3 contents, even closing to zero. The excellent dielectric characteristics of the $0.92 \cdot (\text{Mg}_{0.95}\text{Ni}_{0.05})_2\text{TiO}_4 \cdot 0.08\text{CaTiO}_3$ sintered at 1350 °C was presented with an ϵ_r of 19.2, an Qf of 108,200 GHz, and a τ_f of -4.8 ppm/°C. Therefore, the CaTiO_3 -modified $(\text{Mg}_{0.95}\text{Ni}_{0.05})_2\text{TiO}_4$ ceramic system showed high thermal stability and performance, suggesting the potential of these ceramics as dielectric substrate materials and radio frequency passive components in the microwave field to miniaturize components and transmit signals neglecting the temperature factor.

Author Contributions: C.-H.S. wrote the manuscript and performed the experiment; T.-Y.H., K.-C.L., S.-H.H., C.-H.W. and Y.-T.L. performed the experiment; Z.-L.T. contributed to the analysis the results; Z.-L.T. financially supported the research materials and publication fees; C.-H.S., T.-W.S., W.-F.W. and Z.-L.T. revised the manuscript. All authors have read and agreed to the published version of the manuscript.

Funding: This research received no external funding.

Conflicts of Interest: The authors declare no conflict of interest.

References

1. Freitas, A.E.; Manhabosco, T.M.; Batista, R.J.C.; Segundo, A.K.R.; Araújo, H.X.; Araújo, F.G.S.; Costa, A.R. Development and Characterization of Titanium Dioxide Ceramic Substrates with High Dielectric Permittivities. *Materials* **2020**, *13*, 386. [[CrossRef](#)] [[PubMed](#)]
2. Aljaafari, A.; Sedky, A. Influence of Fine Crystal Percentage on the Electrical Properties of ZnO Ceramic-Based Varistors. *Crystals* **2020**, *10*, 681. [[CrossRef](#)]
3. Yu, H.; Luo, T.; He, L.; Liu, J. Effect of ZnO on Mg₂TiO₄–MgTiO₃–CaTiO₃ Microwave Dielectric Ceramics Prepared by Reaction Sintering Route. *Adv. Appl. Ceram.* **2019**, *118*, 98–105. [[CrossRef](#)]
4. Zhai, S.; Liu, P.; Fu, Z. Microwave Dielectric Properties of Low-Fired [Mg_{0.98}(Li_{0.5}Bi_{0.5})_{0.02}]₂SiO₄–Ca_{0.8}Sm_{0.4/3}TiO₃ Composite Ceramics. *J. Mater. Sci. Mater. Electron.* **2018**, *29*, 1298–1303. [[CrossRef](#)]
5. Palmero, P. Structural Ceramic Nanocomposites: A Review of Properties and Powders' Synthesis Methods. *Nanomaterials* **2015**, *5*, 656–696. [[CrossRef](#)]
6. Tang, B.; Xiang, Q.; Fang, Z.; Zhang, X.; Xiong, Z.; Li, H.; Yuan, C.; Zhang, S. Influence of Cr³⁺ Substitution for Mg²⁺ on the Crystal Structure and Microwave Dielectric Properties of CaMg_{1-x}Cr_{2x/3}Si₂O₆ Ceramics. *Ceram. Int.* **2019**, *45*, 11484–11490. [[CrossRef](#)]
7. Yuan, S.; Gan, L.; Ning, F.; An, S.; Jiang, J.; Zhang, T. High-Q×f 0.95 MgTiO₃–0.05CaTiO₃ Microwave Dielectric Ceramics with the Addition of LiF Sintered at Medium Temperatures. *Ceram. Int.* **2018**, *44*, 20566–20569. [[CrossRef](#)]
8. Gogoi, P.; Singh, L.R.; Pamu, D. Characterization of Zn Doped MgTiO₃ Ceramics: An Approach for RF Capacitor Applications. *J. Mater. Sci. Mater. Electron.* **2017**, *28*, 11712–11721. [[CrossRef](#)]
9. Ullah, A.; Iqbal, Y.; Mahmood, T.; Mahmood, A.; Naem, A.; Hamayun, M. Kinetic Analysis on the Synthesis of Mg_{0.95}Zn_{0.05}TiO₃ Microwave Dielectric Ceramic by Polymeric Precursor Method. *Ceram. Int.* **2015**, *41*, 15089–15096. [[CrossRef](#)]
10. Huang, C.L.; Pan, C.L.; Hsu, J.F. Dielectric Properties of (1–x)(Mg_{0.95}Co_{0.05})TiO₃–xCaTiO₃ Ceramic System at Microwave Frequency. *Mater. Res. Bull.* **2002**, *37*, 2483–2490. [[CrossRef](#)]
11. Sohn, J.H.; Inaguma, Y.; Yoon, S.O.; Itoh, M.; Nakamura, T.; Yoon, S.J.; Kim, H.J. Microwave Dielectric Characteristics of Ilmenite-Type Titanates with High Q Values. *Jpn. J. Appl. Phys.* **1994**, *33*, 5466. [[CrossRef](#)]
12. Wakino, K. Recent Development of Dielectric Resonator Materials and Filters in Japan. *Ferroelectrics* **1989**, *91*, 69–86. [[CrossRef](#)]
13. Isobe, M.; Ueda, Y. Synthesis, Structure and Physical Properties of Spinel Solid Solutions Mg₂TiO₄–MgTi₂O₄. *J. Alloy. Compd.* **2004**, *383*, 85–88. [[CrossRef](#)]
14. Belous, A.; Ovchar, O.; Durilin, D.; Krzmann, M.M.; Valant, M.; Suvorov, D. High-Q Microwave Dielectric Materials Based on the Spinel Mg₂TiO₄. *J. Am. Ceram. Soc.* **2006**, *89*, 3441–3445. [[CrossRef](#)]
15. Belous, A.; Ovchar, O.; Durylin, D.; Valant, M.; Macek-Krzmann, M.; Suvorov, D. Microwave Composite Dielectrics Based on Magnesium Titanates. *J. Eur. Ceram. Soc.* **2007**, *27*, 2963–2966. [[CrossRef](#)]
16. Shannon, R.D. Revised Effective Ionic Radii and Systematic Studies of Interatomic Distances in Halides and Chalcogenides. *Acta Cryst. A* **1976**, *32*, 751–767. [[CrossRef](#)]
17. Huang, C.L.; Ho, C.E. Microwave Dielectric Properties of (Mg_{1-x}Ni_x)₂TiO₄ (x=0.02–0.1) Ceramics. *Int. J. Appl. Ceram. Technol.* **2010**, *7*, E163–E169. [[CrossRef](#)]
18. Petrova, M.A.; Mikirticheva, G.A.; Novikova, A.S.; Popova, V.F. Spinel Solid Solutions in the Systems MgAl₂O₄–ZnAl₂O₄ and MgAl₂O₄–Mg₂TiO₄. *J. Mater. Res.* **1997**, *12*, 2584–2588. [[CrossRef](#)]
19. Shen, C.H.; Pan, C.L.; Lin, S.H. A Study of the Effect of Sintering Conditions of Mg_{0.95}Ni_{0.05}Ti₃ on Its Physical and Dielectric Properties. *Molecules* **2020**, *25*, 5988. [[CrossRef](#)]
20. Huang, C.L.; Liu, S.S. Dielectric Characteristics of the (1–x)Mg₂TiO₄–xSrTiO₃ Ceramic System at Microwave Frequencies. *J. Alloy. Compd.* **2009**, *471*, L9–L12. [[CrossRef](#)]
21. Huang, C.L.; Wang, J.J.; Chang, Y.P. Dielectric Properties of Low Loss (1–x)(Mg_{0.95}Zn_{0.05})TiO₃–xSrTiO₃ Ceramic System at Microwave Frequency. *J. Am. Ceram. Soc.* **2007**, *90*, 858–862. [[CrossRef](#)]
22. Huang, C.L.; Liu, S.S.; Chen, S.H. Dielectric Properties of a New Ceramic System (Mg_{0.95}Zn_{0.05})₂TiO₄–CaTiO₃ at Microwave Frequencies. *Jpn. J. Appl. Phys.* **2009**, *48*, 071402. [[CrossRef](#)]
23. Huang, C.L.; Chen, J.Y. Low-Loss Microwave Dielectrics Using SrTiO₃-Modified (Mg_{0.95}Co_{0.05})₂TiO₄ Ceramics. *J. Alloy. Compd.* **2009**, *485*, 706–710. [[CrossRef](#)]
24. Shen, C.H.; Pan, C.L. Dielectric Properties and Applications of Low-Loss (1–x)(Mg_{0.95}Ni_{0.05})₂TiO₄–xSrTiO₃ Ceramic System at Microwave Frequency. *Int. J. Appl. Ceram. Technol.* **2015**, *12*, E127–E133. [[CrossRef](#)]

25. Kobayashi, Y.; Katoh, M. Microwave Measurement of Dielectric Properties of Low-Loss Materials by the Dielectric Rod Resonator Method. *IEEE Trans. Microw. Theory Tech.* **1985**, *33*, 586–592. [[CrossRef](#)]
26. Courtney, W.E. Analysis and Evaluation of a Method of Measuring the Complex Permittivity and Permeability Microwave Insulators. *IEEE Trans. Microw. Theory Tech.* **1970**, *18*, 476–485. [[CrossRef](#)]
27. Hakki, B.W.; Coleman, P.D. A Dielectric Resonator Method of Measuring Inductive Capacities in the Millimeter Range. *IRE Trans. Microw. Theory Tech.* **1960**, *8*, 402–410. [[CrossRef](#)]
28. Silverman, B.D. Microwave Absorption in Cubic Strontium Titanate. *Phys. Rev.* **1962**, *125*, 1921–1930. [[CrossRef](#)]

Disclaimer/Publisher’s Note: The statements, opinions and data contained in all publications are solely those of the individual author(s) and contributor(s) and not of MDPI and/or the editor(s). MDPI and/or the editor(s) disclaim responsibility for any injury to people or property resulting from any ideas, methods, instructions or products referred to in the content.